

Exact solution of stagnation point flow of MHD Cu–H₂O nanofluid induced by an exponential stretching sheet with thermal conductivity

I Rashid¹, M Sagheer and S Hussain

Department of Mathematics, Capital University of Science and Technology, Islamabad, Pakistan

E-mail: mehar.irfan014@gmail.com

Received 26 June 2019, revised 29 August 2019

Accepted for publication 13 September 2019

Published 23 January 2020



CrossMark

Abstract

This study presents the stagnation point boundary layer flow of copper–water based nanofluid subject to the applied magnetic field. The flow is caused by the presence of an exponentially stretching porous wall. Heat transfer analysis is also taken into account along with the thermal radiation and Joule heating effects. Mathematical modeling is performed to convert the physical system into a set of mathematical equations which are further simplified by using suitable variables. Exact solutions for the velocity and temperature profiles are computed and interpreted for various physical parameters of interest. It is observed that by increasing the magnitude of the solid volume fraction of nanoparticles, the velocity profile is accelerated. The results also indicate an increment in the Eckert number increases the temperature and the thermal boundary layer thickness.

Keywords: nanofluid, thermal radiations, magnetic field, prescribed surface temperature, exact solution, shape factor

(Some figures may appear in colour only in the online journal)

1. Introduction

In recent years, the interest of engineers and mathematicians is focused on the valuable and fascinating applications of copper nanoparticles in medical, chemical, and in engineering industry. Few of these applications are: copper nanoparticles acts as an anti-biotic, anti-microbial, anti-fungal agent when added to plastics, coatings, textiles, high strength metals, heat sinks, highly thermal conductive materials, electronics, and displays. The basic purpose of nanoparticles is to enhance the thermal abilities of base fluid. Because conventional heat transfer fluids, including oil, water, and ethylene glycol mixture are poor heat transfer fluids, since the thermal conductivity of these fluids plays an important role on the heat transfer coefficient between the heat transfer medium and the heat transfer surface. Dramatic heat transfer and high thermo physical properties of nanofluids make them significant in

research field in recent years. Nanofluids play key role in many industries such as in power generators, micro-electro-mechanical systems, microprocessors and biotechnology (particularly for drug delivery). Choi [1] in 1995 first time incorporate the nano materials in the conventional fluids and termed it as nanofluids. After which many researchers investigated nanofluids experimentally and theoretically [2–5]. Nield and Kuznetsov [6] previously studied the flat surface nanofluid system to find the combined effect of Brownian motion and thermophoresis on the boundary layer flow. Kakac and Pramuanjaroenkij [7] investigated nanofluids for their convective transport. Maxwell model for nanofluids was applied by Srinivas and Vinod [8] to explore the influence of heat generation or absorption on the boundary layer flow. Recently more advance and relevant study on nanofluids was carried out [9–16].

Stretching surfaces under the influence of magnetic field is a topic of great interest because of its potential applications in engineering and industrial processes such as crystal

¹ Author to whom any correspondence should be addressed.

growing, manufacturing of paper, glass fiber drawing, generation of plasma, geothermal and petroleum industries. Crane first time [17] gives the idea of boundary layer flow of viscous incompressible fluid produced by a stretching surface in 1970. Later on, Anderson *et al* [18] presented the study of the magnetohydrodynamic viscous flow on a linear stretching surface. Wang [19] studied the Newtonian flow induced by a stretching surface with slip and suction effects. Andersson *et al* [20] investigated an exact analytical solution for slip flow over a stretching surface. Fang *et al* [21] examined the MHD flow of viscous fluid under a slip condition past a stretching surface. Later on various researchers used the philosophy of Crane with more innovative ideas such as nonlinearly and exponentially stretching surfaces, which was found very useful in industrial and engineering processes. In this regard, Alinejad and Samarbakhsh [22] studied the flow of Newtonian fluid past a nonlinear stretching plate with viscous dissipation phenomenon. Kumbhakar and Rao [23] studied the boundary layer flow of thermally radiating surface over a nonlinear stretching sheet. Seth and Mishra [24] analyzed the transient flow of nanofluid induced by a nonlinear stretching sheet. Jayarami *et al* [25] investigated the mixed convective flow of chemically reactive Cassion fluid past a nonlinear stretching. Magyari and Keller [26] investigated the exponential temperature distribution past an exponentially stretching surface. Elbashbeshy [27] examined the effects of suction on laminar flow over an exponentially stretching surface. El-Aziz [28] studied the mixed convective flow of micro-rotating fluid driven by an exponentially stretching surface. Mandal and Mukhopadhyay [29] studied the mixed convection flow of micro-rotating fluid with fluid friction phenomenon induced by an exponentially stretching surface.

To our knowledge, the stagnation point boundary layer flow of copper–water based nanofluid subject to the magnetic field due to an exponentially stretching porous wall is still not investigated. Further, the thermal radiation and the Joule heating effects are also taken into consideration in the energy equation as a body force. Analytical solutions are attained for the momentum and heat equations adopting confluent hypergeometric function of 1st kind which is known as Kummer’s function. Graphical results are prepared and portrayed to analyze the emerging parameters behavior. The coefficient of local Nusselt number and local skin friction are perused through numerical computations and graphs.

2. Problem statement

A steady, two dimensional, incompressible flow of Cu–water nanofluid passed a permeable exponentially stretching sheet has been considered. The x -axis is taken along the stretching sheet in the direction of flow and y -axis is considered normal to the flow direction can be seen in figure 1. The fluid occupies the space $y > 0$. The sheet is stretched in the x -direction with a velocity $u = u_0 e^{x/L}$. Moreover, the magnetic field B_0 is applied normal to the fluid flow. Effects of Joule heating and thermal radiation phenomena are further examined in the energy equation. The elementary equations

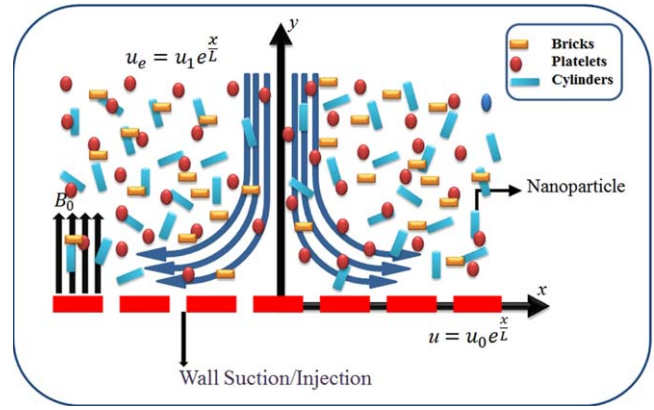


Figure 1. Geometry of the problem.

governing the two dimensional MHD flow are:

$$\frac{\partial u}{\partial x} + \frac{\partial v}{\partial y} = 0, \tag{1}$$

$$u \frac{\partial u}{\partial x} + v \frac{\partial v}{\partial y} = \frac{\mu_{nf}}{\rho_{nf}} \frac{\partial^2 u}{\partial y^2} + \frac{\mu_{nf}}{\rho_{nf} k} (u_e - u) + u_e \frac{\partial u_e}{\partial x} - \frac{\sigma_{nf} B(x)^2}{\rho_{nf}} u, \tag{2}$$

where u, v represent the velocity components along x - and y -directions respectively, $B(x)$ the magnetic parameter, ρ_{nf} the density, μ_{nf} the dynamic viscosity, α_{nf} the thermal diffusivity, ν_{nf} the kinematic viscosity, $(\rho c_p)_{nf}$ the specific heat capacitance of the nanofluid. Hamilton and Crosser model (1962) to consider different shaped particle by presenting a shape factor. As per this model, when the thermal conductivity of the nanoparticles is 100 times bigger than that of the host fluid, the thermal conductivity can be shown as:

$$\left. \begin{aligned} \mu_{nf} &= \frac{\mu_{nf}}{(1 - \phi)^{2.5}}, & \alpha_{nf} &= \frac{k_{nf}}{(\rho c_p)_{nf}}, \\ (\rho c_p)_{nf} &= (1 - \phi)(\rho c_p)_f + \phi(\rho c_p)_s, \\ \nu_{nf} &= \frac{\mu_{nf}}{\rho_{nf}}, & \rho_{nf} &= (1 - \phi)\rho_f + \phi(\rho_s), \\ \frac{k_{nf}}{k_f} &= \frac{(k_s + (m + 1)k_f) - (m + 1)\phi(k_f - k_s)}{(k_s + (m + 1)k_f) + \phi(k_f - k_s)}, \\ \frac{\sigma_{nf}}{\sigma_f} &= 1 + \frac{3\left(\frac{\sigma_{nf}}{\sigma_f} - 1\right)\phi}{\left(\frac{\sigma_{nf}}{\sigma_f} + 2\right) - \left(\frac{\sigma_{nf}}{\sigma_f} - 1\right)\phi}, \end{aligned} \right\} \tag{3}$$

In the above equations, ρ_f and $(\rho c_p)_f$ are the density and the effective heat capacity of the host fluid, ϕ the solid volume fraction, σ_f and σ_{nf} expressed the electrical conductivity of the host and nanofluid, k_f the thermal conductivity of host fluid, k_{nf} the thermal conductivity of nanoparticles. The suitable boundary conditions for the problem defined above are [30]:

$$\left. \begin{aligned} u &= u_0 e^{x/L}, & v &= v_w & \text{at } y &= 0, \\ u &\rightarrow u_e = u_1 e^{x/L} & & & \text{as } y &\rightarrow \infty. \end{aligned} \right\} \tag{4}$$

To non-dimensionalize the variables, following similarity variables have been introduced [30].

$$u = u_0 e^{x/L} f', \quad v = -\left(\frac{u_0 \nu_f}{2L}\right)^{1/2} e^{x/2L} (f + \eta f'),$$

$$\eta = y \left(\frac{u_0}{2\nu L}\right)^{1/2} e^{x/2L}. \tag{5}$$

After using equation (5), the equations (2) is reduced to

$$f''' + A_1 A_2 f f'' + K(A - f') - 2A_1 A_2 f'^2 - A_1 M_2 f' + 2A_1 A_2 A^2 = 0, \tag{6}$$

subject to the boundary conditions:

$$\left. \begin{aligned} f(\eta) = S, \quad f'(\eta) = 1, \quad \text{at } \eta = 0, \\ f'(\eta) \rightarrow \frac{u_e}{u_0} = A \quad \text{as } \eta \rightarrow \infty. \end{aligned} \right\} \tag{7}$$

In the above equations (6) and (7), u_0 represents the reference velocity, u_e the stagnation-point flow velocity, $M_2 = \frac{2L\sigma B_0^2}{\rho}$ the Hartmann number and $K = \frac{u_0 k_0}{L\nu_f}$ the permeability parameter.

Furthermore $S = -\left(\frac{2L}{u_0 \nu_f}\right)^{1/2} e^{-x/2L} v_w$, $A_2 = \left(1 - \phi + \phi \frac{\rho}{\rho_f}\right)$ and $A_1 = (1 - \phi)^{2.5}$. Chakrabarti and Gupta [31] acquired the analytical solution for these type of 3rd order nonlinear differential equations.

$$f(\eta) = a + b e^{-\lambda \eta}. \tag{8}$$

By using equation (7) in (8), We obtain

$$f(\eta) = S + \left(\frac{1 - e^{-\lambda \eta}}{\lambda}\right). \tag{9}$$

By using equation (9) in equation (6), we have

$$\lambda = A_1 A_2 S + \frac{1}{2} \sqrt{A_1^2 A_2^2 S^2 - 8A^2 A_1 A_2 - 4AK + 8A_1 A_2 + A_1 M_2 + 4K}, \tag{10}$$

using in equation (9), one have

$$a = S + \frac{1}{A_1 A_2 S + \frac{1}{2} \sqrt{A_1^2 A_2^2 S^2 - 8A^2 A_1 A_2 - 4AK + 8A_1 A_2 + A_1 M_2 + 4K}}, \tag{11}$$

$$b = -\frac{1}{A_1 A_2 S + \frac{1}{2} \sqrt{A_1^2 A_2^2 S^2 - 8A^2 A_1 A_2 - 4AK + 8A_1 A_2 + A_1 M_2 + 4K}}, \tag{12}$$

where a , b and λ are constants with $\lambda > 0$. Now, using the above constant in equation (9), we get the following velocity profile

$$f(\eta) = S + \left\{ \frac{1}{A_1 A_2 S + \frac{1}{2} \sqrt{A_1^2 A_2^2 S^2 - 8A^2 A_1 A_2 - 4AK + 8A_1 A_2 + A_1 M_2 + 4K}} \right\} \left(1 - e^{-\left(A_1 A_2 S + \frac{1}{2} \sqrt{A_1^2 A_2^2 S^2 - 8A^2 A_1 A_2 - 4AK + 8A_1 A_2 + A_1 M_2 + 4K}\right) \eta} \right), \tag{13}$$

the local skin friction is expressed as

$$C_f = \frac{\tau_w}{\rho u_w^2} = \frac{Re_x^{-1/2}}{A_1} f''(0), \quad A_1 C_f Re_x^{-1/2} = f''(0). \tag{14}$$

In the above equation (14), $\tau_w = \mu_n f \left(\frac{\partial u}{\partial y}\right)_{y=0}$ is the stress at wall and $Re_x = \frac{x u_w}{\nu}$ the Reynolds number.

3. Heat transfer analysis

In this segment, the Heat transfer analysis in the presence of the thermal radiation and Joule heating phenomena has been presented. The elementary equation is given below:

$$u \frac{\partial T}{\partial x} + v \frac{\partial T}{\partial y} = \alpha_{nf} \frac{\partial^2 T}{\partial y^2} - \frac{1}{(\rho C_p)_{nf}} \frac{\partial q_r}{\partial y} + \frac{\sigma_{nf} B(x)^2}{(\rho C_p)_{nf}} u^2, \tag{15}$$

where

$$q_r = -\frac{\sigma^*}{3k^*} \frac{\partial T^4}{\partial y}. \tag{16}$$

Here α_{nf} the thermal diffusivity, T express the temperature field, $(C_p)_{nf}$ the specific heat, k^* denote the mass absorption coefficient and σ^* the Stefan–Boltzmann constant. Using equation (16) into equation (15), we get

$$u \frac{\partial T}{\partial x} + v \frac{\partial T}{\partial y} = \alpha_{nf} \frac{\partial^2 T}{\partial y^2} + \frac{1}{3(\rho C_p)_{nf}} \frac{16\sigma^* T_\infty^3}{k^*} \frac{\partial^2 T}{\partial y^2} + \frac{\sigma_{nf} B(x)^2}{(\rho C_p)_{nf}} u^2. \tag{17}$$

The boundary conditions have been taken as

$$\left. \begin{aligned} T = T_w = T_\infty + T_0 e^{x/L} \quad \text{at } y = 0, \\ T \rightarrow T_\infty \quad \text{as } y \rightarrow \infty, \end{aligned} \right\} \tag{18}$$

where T_0 expresses the constant reference temperature, L the characteristic length, T_w the temperature of the sheet and T_∞ represents the free stream temperature. The similarity variable for the temperature field is given as [30]:

$$\theta(\eta) = \frac{T - T_\infty}{T_w - T_\infty}. \tag{19}$$

The following dimensionless energy equation is obtained after utilizing the similarity variables defined in equations (5)

and (19)

$$\omega \theta'' + Pr f \theta' - 2 Pr f' \theta + \frac{Pr M_2}{A_4} Ec f'' = 0, \quad (20)$$

where

$$\begin{aligned} Ec &= \frac{u^2}{(T_w - T_\infty) Cp}, \quad Pr = \frac{\nu_f}{\alpha_f}, \\ N &= \frac{K^* K_f}{4 \sigma^* T_\infty^3}, \quad \omega = \left(\frac{A_3}{A_4} \frac{3NA_3 + 4}{3NA_3} \right) \\ A_3 &= \frac{(k_s + 2k_f) - 2\phi(k_f - k_s)}{(k_s + 2k_f) + 2\phi(k_f - k_s)}, \\ A_4 &= \left(1 - \phi + \phi \frac{(\rho Cp)_s}{(\rho Cp)_f} \right). \end{aligned} \quad (21)$$

Here Ec the Eckert number, N the radiation parameter and Pr the Prandtl number. The reduced boundary condition are:

$$\left. \begin{aligned} \theta(\eta) &= 1 & \text{at} & \quad \eta = 0, \\ \theta(\eta) &\rightarrow 0 & \text{as} & \quad \eta \rightarrow \infty. \end{aligned} \right\} \quad (22)$$

Now, putting equation (9) into (20), it is easy to get

$$\begin{aligned} w \theta_{\eta\eta} + Pr \left(S + \frac{1}{\lambda} \left(\frac{1 - e^{-\lambda\eta}}{\lambda} \right) \right) \theta_\eta \\ - 2 Pr e^{-\lambda\eta} \theta + \frac{Pr M_2}{A_4} Ec (e^{-\lambda\eta})^2 = 0. \end{aligned} \quad (23)$$

Any linear differential equation of second order can be reduced to Kummer's ordinary differential equation. For this purpose new variable is introduced

$$\xi = -\frac{Pr e^{-\lambda\eta}}{\omega \lambda^2}. \quad (24)$$

As a result equation (23) becomes Kummer's ordinary differential equation:

$$\xi \frac{\partial^2 \theta}{\partial \xi^2} + (h - \xi) \frac{\partial \theta}{\partial \xi} - g \theta = -\frac{Pr M_2}{A_4} Ec (e^{-\lambda\eta})^2, \quad (25)$$

where $h = (1 - P)$, $P = \frac{Pr}{\omega \lambda} \left(S + \frac{1}{\lambda} \right)$ and $g = -2$. The boundary conditions are taken as

$$\theta(\xi) = 1, \quad \theta(0) = 0. \quad (26)$$

The exact solution of equation (25) with (26) in terms of Kummer's functions [32], is

$$\left. \begin{aligned} \theta(\xi) &= \left(\frac{\xi^{\frac{Pr}{\omega \lambda} \left(S + \frac{1}{\lambda} \right)} M \left(-2 + \frac{Pr}{\omega \lambda} \left(S + \frac{1}{\lambda} \right), 1 + \frac{Pr}{\omega \lambda} \left(S + \frac{1}{\lambda} \right), \xi \right)}{2 \left(-\frac{Pr}{\omega \lambda^2} \right)^{\frac{Pr}{\omega \lambda} \left(S + \frac{1}{\lambda} \right)} M \left(-2 + \frac{Pr}{\omega \lambda} \left(S + \frac{1}{\lambda} \right), 1 + \frac{Pr}{\omega \lambda} \left(S + \frac{1}{\lambda} \right), -\frac{Pr}{\omega \lambda^2} \right)} \right) \\ &\times \left(\frac{1}{(\omega \lambda^2 A_4) \left(-2 + \frac{Pr}{\omega \lambda} \left(S + \frac{1}{\lambda} \right) \right)} \right) \\ &+ \left(\frac{Pr}{\omega \lambda} \left(S + \frac{1}{\lambda} \right)^2 + (-\xi - 3) \frac{Pr}{\omega \lambda} \left(S + \frac{1}{\lambda} \right) + \xi^2 - 4 + 2 \right) \\ &\times \left(\frac{M_2 Ec \omega \lambda^2}{2 A_4 Pr \left(-2 + \frac{Pr}{\omega \lambda} \left(S + \frac{1}{\lambda} \right) \right)} - M_2 Ec \omega \lambda^2 \frac{2\xi - 1 + \frac{Pr}{\omega \lambda} \left(S + \frac{1}{\lambda} \right)}{2 A_4 Pr} \right), \end{aligned} \right\} \quad (27)$$

In the above equation (27), M represents the confluent hypergeometric function of 1st kind. The Kummer function of equation (27) are defined as follows

$$\left. \begin{aligned} \theta(\eta) &= \left(\frac{e^{-\lambda \frac{Pr}{\omega \lambda} \left(S + \frac{1}{\lambda} \right)} Pr \eta M \left(-2 + \frac{Pr}{\omega \lambda} \left(S + \frac{1}{\lambda} \right), 1 + \frac{Pr}{\omega \lambda} \left(S + \frac{1}{\lambda} \right), -\frac{Pr}{\omega \lambda^2} e^{-\lambda\eta} \right)}{2 M \left(-2 + \frac{Pr}{\omega \lambda} \left(S + \frac{1}{\lambda} \right), 1 + \frac{Pr}{\omega \lambda} \left(S + \frac{1}{\lambda} \right), -\frac{Pr}{\omega \lambda^2} \right)} \right) \\ &\times \left(\frac{1}{(\omega \lambda^2 A_4) \left(-2 + \frac{Pr}{\omega \lambda} \left(S + \frac{1}{\lambda} \right) \right)} \right) \\ &+ \left(\frac{Pr}{\omega \lambda} \left(S + \frac{1}{\lambda} \right)^2 + \left(-\frac{Pr}{\omega \lambda^2} e^{-\lambda\eta} - 3 \right) \frac{Pr}{\omega \lambda} \left(S + \frac{1}{\lambda} \right) \right. \\ &+ \left. \left(\frac{Pr}{\omega \lambda^2} e^{-\lambda\eta} \right)^2 - 4 \frac{Pr}{\omega \lambda^2} e^{-\lambda\eta} + 2 \right) \\ &\times \left(\frac{M_2 Ec \omega \lambda^2}{2 A_4 Pr \left(-2 + \frac{Pr}{\omega \lambda} \left(S + \frac{1}{\lambda} \right) \right)} - M_2 Ec \omega \lambda^2 \frac{2\xi - 1 + \frac{Pr}{\omega \lambda} \left(S + \frac{1}{\lambda} \right)}{2 A_4 Pr} \right). \end{aligned} \right\} \quad (28)$$

$$\left. \begin{aligned} \theta_\eta(0) &= \frac{Pr^2 \left(S + \frac{1}{\lambda} \right)^2 a \left(2 A_4 Pr \lambda \left(S + \frac{1}{\lambda} \right) - 4 A_4 \lambda^2 \omega - M_2 Ec Pr \right)}{2 \omega^2 a A_4 \lambda^2 (-2 + P)} \\ &+ \left(\frac{Pr \left(S + \frac{1}{\lambda} \right) (b - a) \left(2 A_4 Pr \lambda \left(S + \frac{1}{\lambda} \right) - 4 A_4 \lambda^2 \omega - M_2 Ec Pr \right)}{\omega^2 a A_4 \lambda} \right) \\ &- \left(\frac{1}{2 a A_4 \lambda \omega} \left(-(c - b) \left(-1 + \frac{Pr S}{\omega \lambda} + \frac{Pr}{\omega \lambda^2} \right) \lambda \right. \right. \\ &+ \left. \left. (b - a) \right) \right) \left(-2\xi + \frac{Pr S}{\omega \lambda} + \frac{Pr}{\omega \lambda^2} \right) \lambda \\ &\times \left(2 A_4 Pr \lambda \left(S + \frac{1}{\lambda} \right) - 4 A_4 \lambda^2 \omega - M_2 Pr Ec \right) \\ &+ \left(\frac{\left(-\frac{2 Pr}{\omega^2 \lambda} \left(S + \frac{1}{\lambda} \right) + \frac{4 Pr}{\omega} \right) Ec M_2 \lambda^2 \omega}{A_4 Pr \left(-2 + \frac{Pr}{\omega \lambda} \left(S + \frac{1}{\lambda} \right) \right)} + \frac{Ec M_2 \lambda^2}{A_4} \right), \end{aligned} \right\} \quad (29)$$

where

$$\begin{aligned} a &= M \left(-2 + \frac{Pr}{\omega \lambda} \left(S + \frac{1}{\lambda} \right), 1 + \frac{Pr}{\omega \lambda} \left(S + \frac{1}{\lambda} \right), -\frac{Pr}{\lambda^2 \omega} \right), \\ b &= M \left(-1 + \frac{Pr}{\omega \lambda} \left(S + \frac{1}{\lambda} \right), 1 + \frac{Pr}{\omega \lambda} \left(S + \frac{1}{\lambda} \right), -\frac{Pr}{\lambda^2 \omega} \right), \\ c &= M \left(\frac{Pr}{\omega \lambda} \left(S + \frac{1}{\lambda} \right), 1 + \frac{Pr}{\omega \lambda} \left(S + \frac{1}{\lambda} \right), -\frac{Pr}{\lambda^2 \omega} \right), \\ \lambda &= A_1 A_2 S \\ &+ \frac{1}{2} \sqrt{A_1^2 A_2^2 S^2 - 8 A^2 A_1 A_2 - 4 A K + 8 A_1 A_2 + A_1 M_2 + 4 K}. \end{aligned}$$

Accordingly, the above equation initiated the non-dimensional wall temperature. The local Nusselt number can be written as:

$$Nu = \frac{-k_{nf} x \left(\frac{\partial T}{\partial y} \right)_{y=0}}{k_f (T_w - T_\infty)} = -\frac{k_{nf}}{k_f} Re_x^{1/2} \theta_\eta(0). \quad (30)$$

In the current study, it is acquired as:

$$\frac{k_f}{k_{nf}} Nu_x Re_x^{-1/2} = -\theta_\eta(0). \quad (31)$$

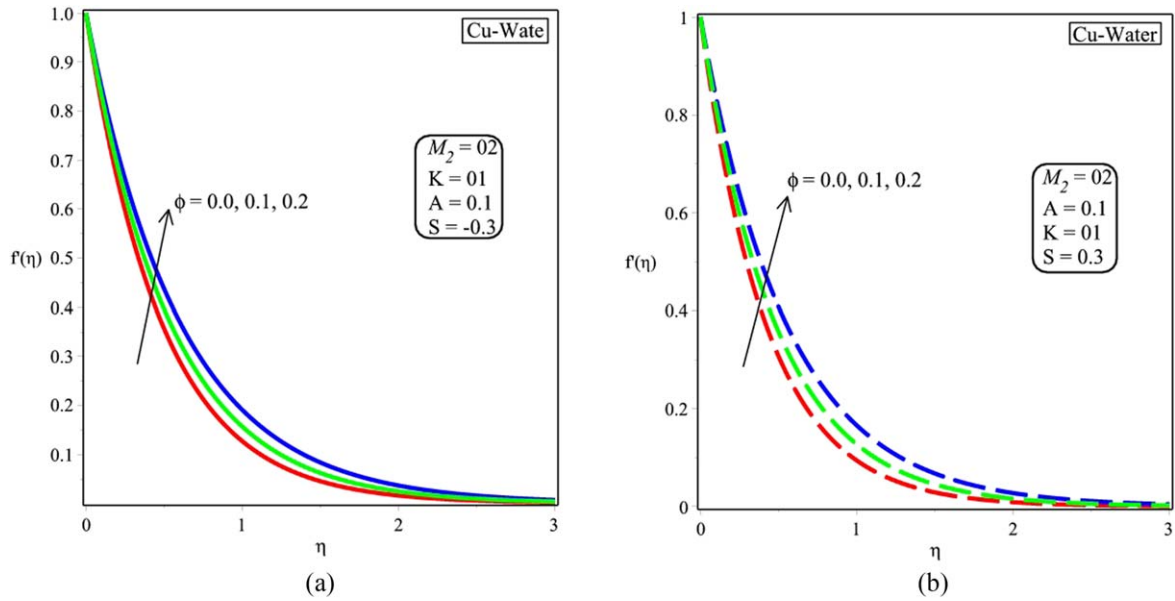


Figure 2. (a) Influence of ϕ ($S = -0.3$) on velocity profiles. (b) Influence of ϕ ($S = 0.3$) on velocity profiles.

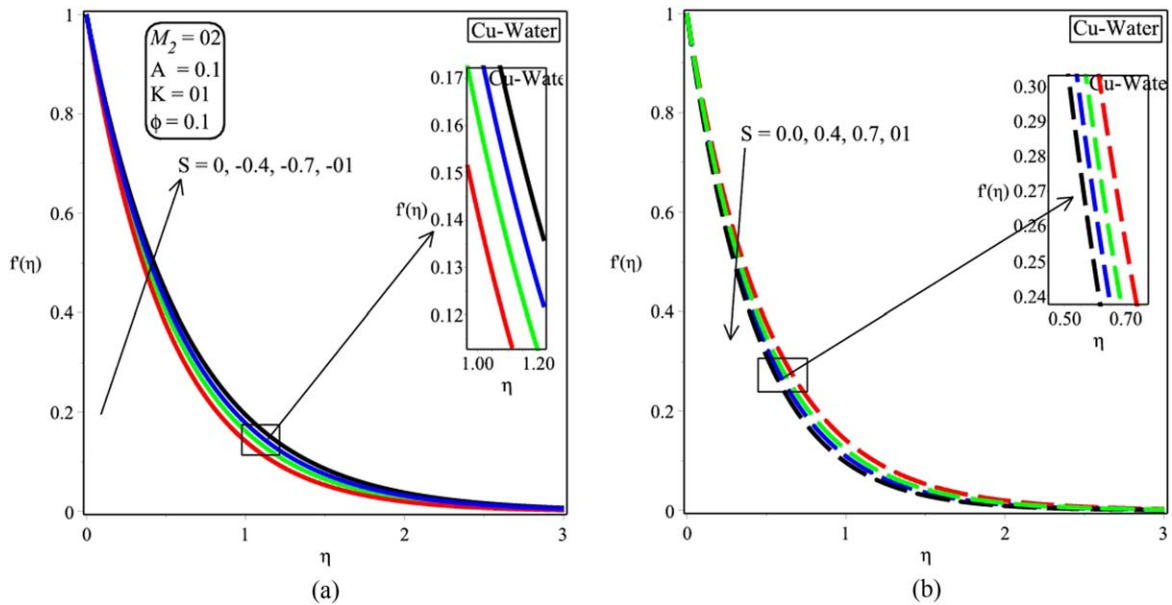


Figure 3. (a) Influence of S (injection) on velocity profiles. (b) Influence of S (suction) on velocity profiles.

4. Results and discussion

In this part, the effect of several emerging parameters on the velocity profiles and temperature profiles has been shown in order to envision the conduct of these parameters. In this regard, figures 2–18 are prepared. The graphs showed in figures 2(a) and (b) are plotted to visualize the behavior of velocity of the nanofluid for the nanoparticle concentration ϕ in the presence of suction and injection phenomena separately, while keeping the other the parameters constant. It is examined in these figures that the velocity profile enhances with an increment in the solid volume fraction. Influence of the suction/injection parameter is depicted in figures 3(a) and (b). It can be seen in figure 3(b) that the velocity profile

increases for the mass blowing ($S < 0$) and a quite opposite behavior of the same profile is recorded for the mass suction ($S > 0$) in figure 3(b). An increment in the velocity ratio parameter $A = \frac{u_e}{u_o}$ strongly accelerates the velocity profile (see figure 4). Moreover, it is also perceived that the boundary layer thickness and velocity rise with an increment in A , while the stretching velocity is higher than the stream velocity. The stagnation point flow is found zero, when velocity ratio parameter is taken zero.

Physical insight of the temperature profile with respect to the mass suction/injection, the Eckert number Ec , permeability parameter K , the Prandtl number Pr , the Hartmann number M_2 , the nanoparticles concentration ϕ and the

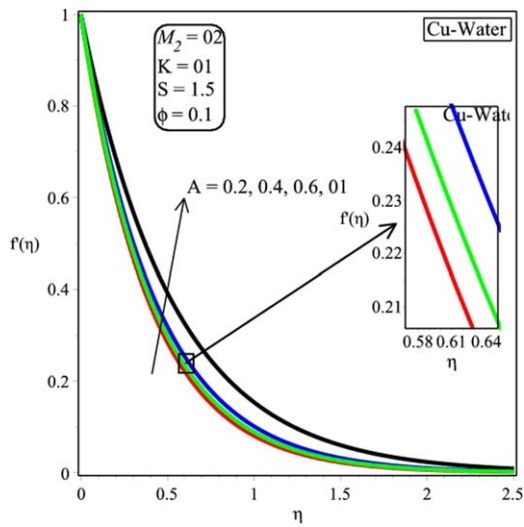


Figure 4. Effect of A on velocity profile.

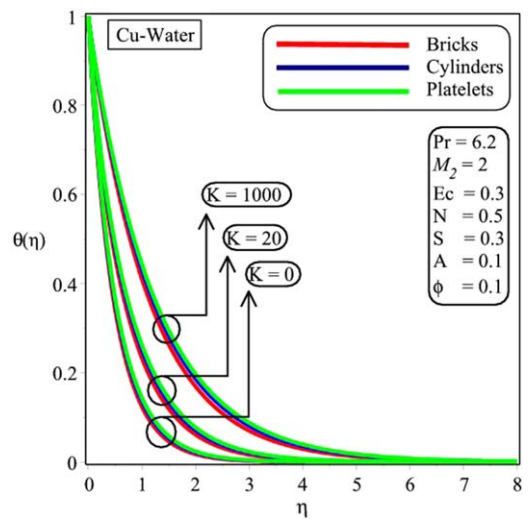


Figure 7. Effect of K on $\theta(\eta)$.

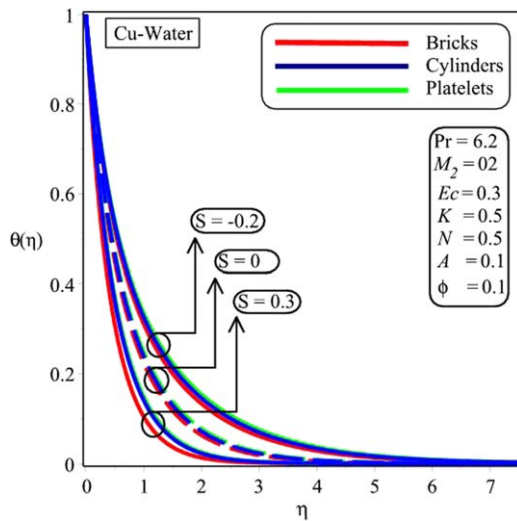


Figure 5. Effect of S on $\theta(\eta)$.

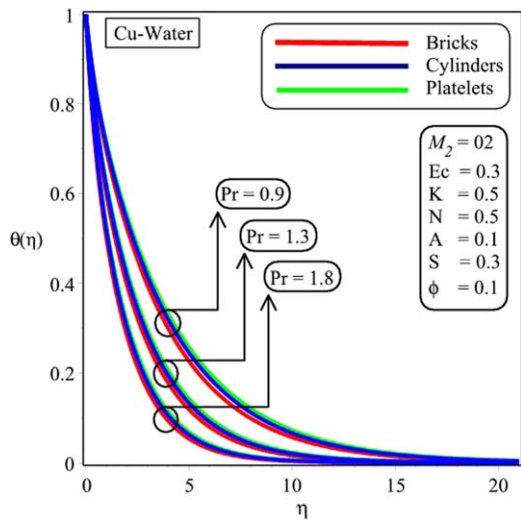


Figure 8. Effect of Pr on $\theta(\eta)$.

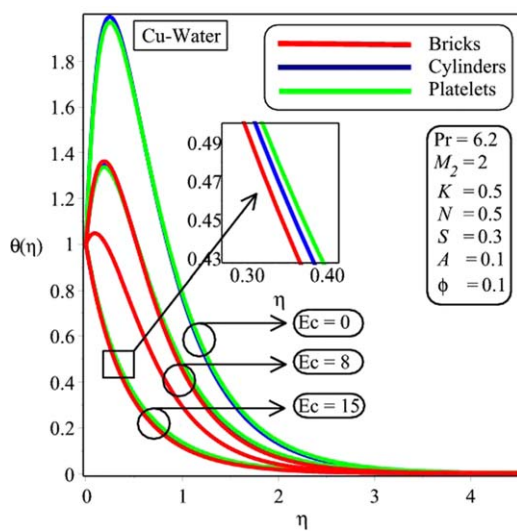


Figure 6. Effect of Ec on $\theta(\eta)$.

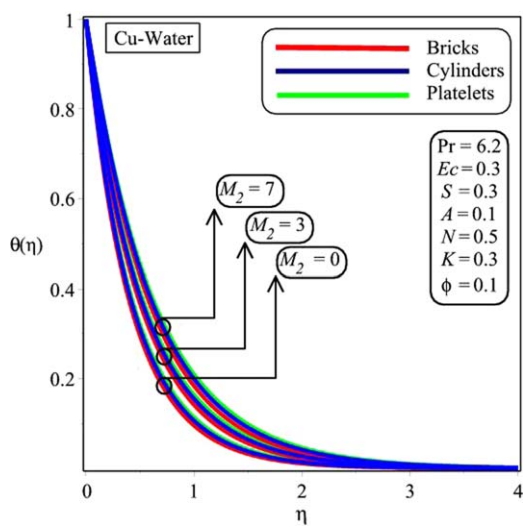


Figure 9. Effect of M_2 on $\theta(\eta)$.

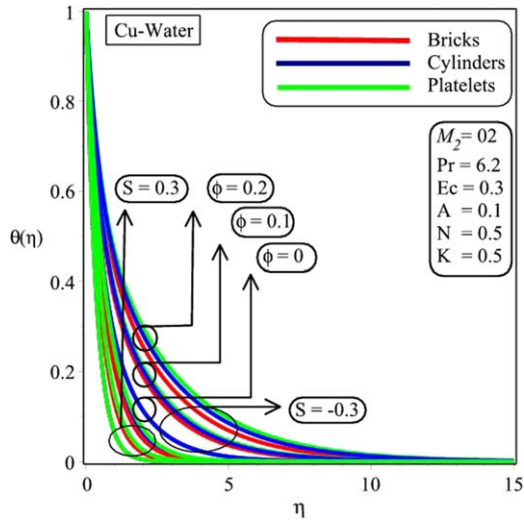


Figure 10. Effect of ϕ on $\theta(\eta)$.

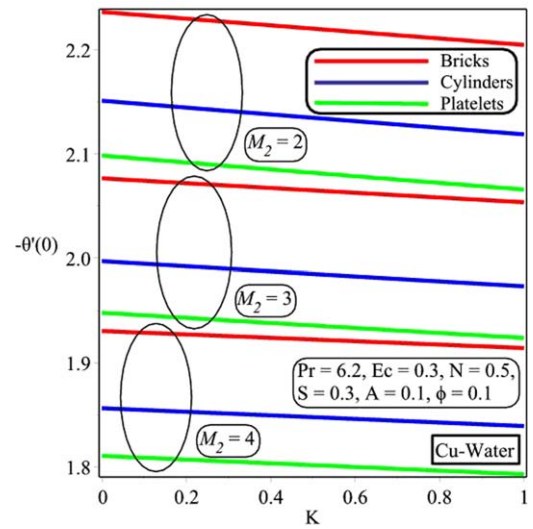


Figure 13. Effect of M_2 on $-\theta'(0)$.

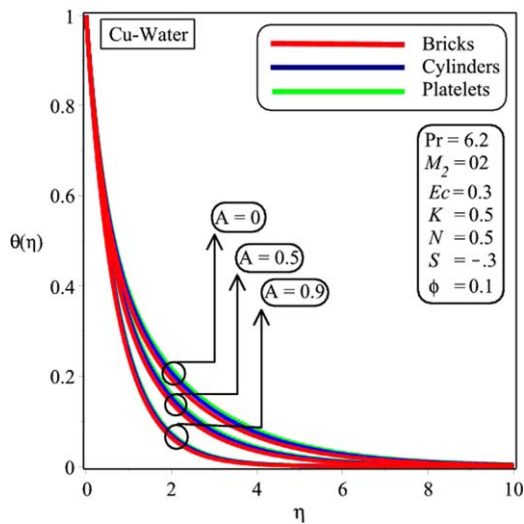


Figure 11. Effect of A on $\theta(\eta)$.

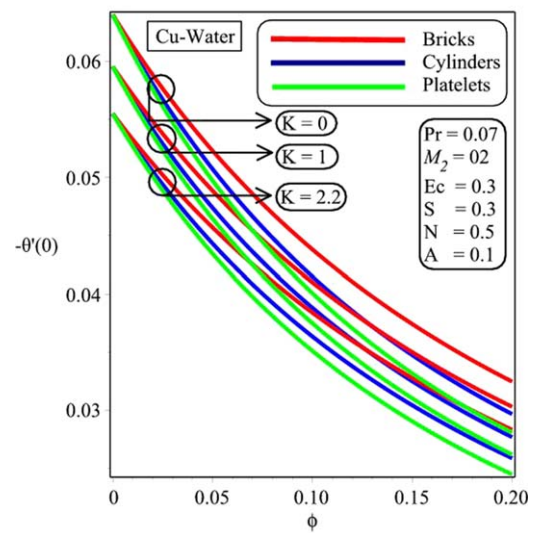


Figure 14. Effect of K on $-\theta'(0)$.

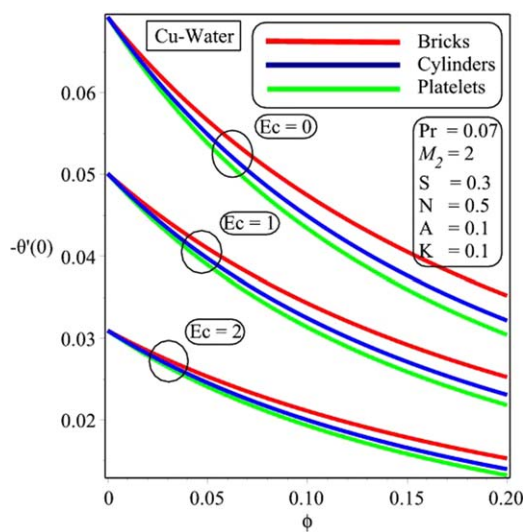


Figure 12. Effect of Ec on $-\theta'(0)$ for $S = 0.3$.

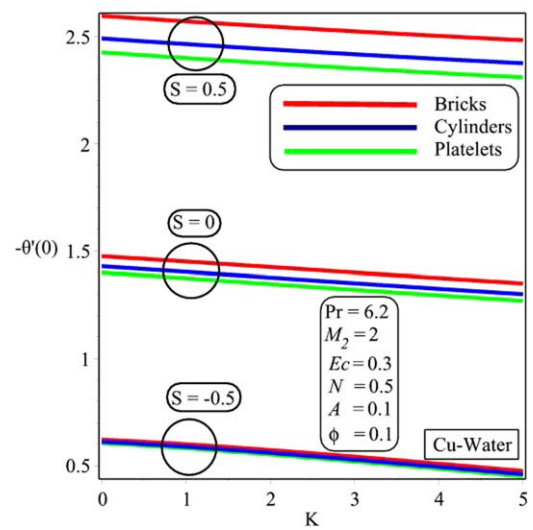


Figure 15. Effect of S on $-\theta'(0)$.

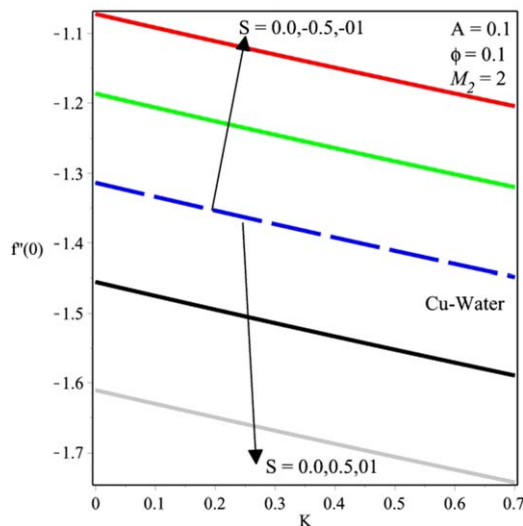


Figure 16. Effect of S on $f''(0)$.

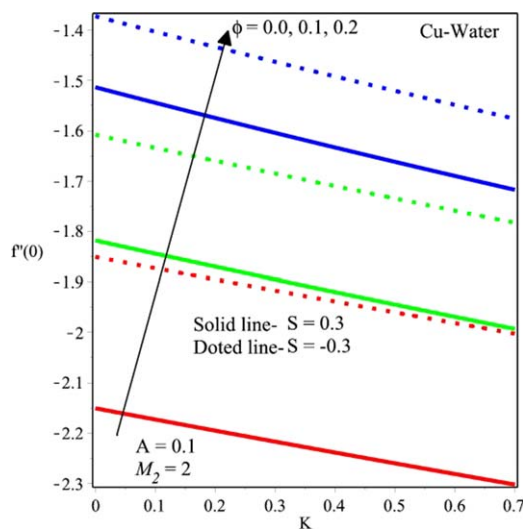


Figure 17. Effect of ϕ on $f''(0)$.

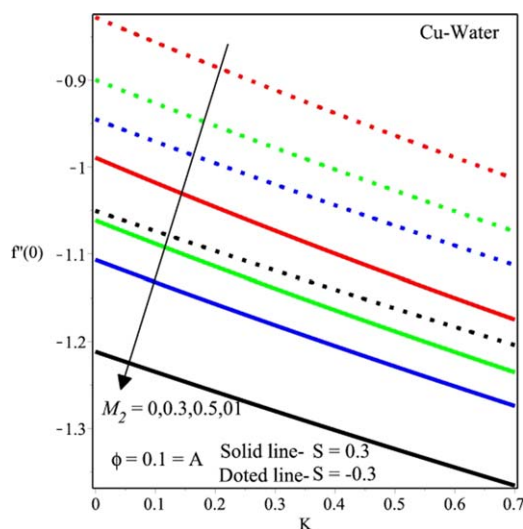


Figure 18. Effects of M_2 on $f''(0)$.

Table 1. Thermophysical properties of host fluids and nanoparticle.

Item		$\frac{\rho}{\text{kg m}^{-3}}$	$\frac{C_p}{\text{J kg}^{-1} \text{K}}$	$\frac{k}{\text{W m}^{-1} \text{K}}$
Base fluid	Water	997	4179	0.613
Nanoparticle	Copper (Cu)	8933	385	400

Table 2. Shape of Nanoparticle with their shape factor is given by Elena et al [33].

Nanoparticles	Shape	Shape factor
Bricks		3.70
Cylinders		4.90
Platelets		5.70

Table 3. Comparison table.

$S > 0$	3.5	4	4.5	5
Bhattacharyya et al [34]	0.666 67	1.000 00	1.228 71	1.434 26
Present study	0.666 67	1.000 00	1.228 71	1.434 26

velocity ratio parameter A are plotted in figures 5–11 respectively. Figure 5 shows the influence of the suction/injection parameter on the temperature profile. The temperature profile decreases for increasing the value of suction parameter. Physically, the effect of suction is to make the temperature distribution more uniform within the boundary layer. Imposition of fluid suction at the surface has a tendency to decrease the thermal boundary layer thickness, which consequently reduces the temperature field. On the other hand, the thermal boundary layer thickness increases with injection which causes a decrease in the rate of heat transfer. Figure 6 portrays the impact of the Eckert number on temperature profile. It is observed that with an increase in the Eckert number there is a gradual decrease in the fluid energy. Here, it is seen that the temperature and thermal boundary-layer thickness increases for increasing values of the Eckert numbers, because heat energy is stored in the liquid due to the frictional heating. Such increase in the Eckert number enhances the temperature at any point in the thermal boundary-layer region. Figure 7 influences the behavior of the permeability parameter on the temperature field. As the permeability of fluid increases there is increase in the fluid temperature, which is obvious. Physically the presence of a

Table 4. Numerical values of the local skin friction coefficient $f''(0)$.

ϕ	A	M_2	S	$K = 0$	0.3	0.5	0.6	0.7
0	0.1	2	0.3	-2.150 62	-2.217 00	-2.260 09	-2.281 31	-2.302 32
0.1				-1.817 98	-1.895 06	-1.944 65	-1.968 95	-1.992 94
0.2				-1.513 48	-1.604 19	-1.661 80	-1.689 83	-1.717 39
0.1	0			-1.822 06	-1.907 31	-1.961 96	-1.988 70	-2.015 25
	0.2			-1.805 67	-1.874 83	-1.919 47	-1.941 38	-1.963 03
	0.3			-1.784 96	-1.846 34	-1.886 09	-1.905 63	-1.924 97
	0.1	0		-1.287 12	-1.396 28	-1.464 20	-1.496 91	-1.528 87
		0.3		-1.380 91	-1.482 66	-1.546 51	-1.577 40	-1.607 65
		0.5		-1.439 78	-1.537 35	-1.598 87	-1.628 69	-1.657 95
		2	-1	-1.395 12	-1.470 83	-1.519 61	-1.543 52	-1.567 14
			-0.5	-1.543 63	-1.620 46	-1.669 90	-1.694 13	-1.718 06
			0	-1.709 73	-1.786 95	-1.836 62	-1.860 96	-1.884 99
			0.5	-1.893 71	-1.970 54	-2.019 99	-2.044 22	-2.068 14
			1	-2.095 29	-2.171 00	-2.219 77	-2.243 69	-2.267 31

Table 5. Numerical values of the local Nusselt number $-\theta'(0)$ for $Ec = 0.3$, $m = 3.7$, $Pr = 6.2$ and $N = 0.5$.

ϕ	A	M_2	S	K	0	0.3	0.5	0.6	0.7
0	0.1	2	0.3		2.845 61	2.837 61	2.832 28	2.829 62	2.826 96
0.1					2.235 92	2.226 24	2.219 88	2.216 72	2.213 59
0.2					1.793 57	1.782 82	1.775 82	1.772 36	1.768 94
0.2			-1		0.793 97	0.780 26	0.770 93	0.766 20	0.761 42
			-0.5		1.030 29	1.013 04	1.001 57	0.995 84	0.990 12
			0		1.452 59	1.438 90	1.429 94	1.425 51	1.421 12
			0.5		2.050 87	2.041 92	2.036 09	2.033 21	2.030 37
			1		2.774 34	2.768 83	2.765 24	2.763 47	2.761 71

A	M_2	K	S	ϕ	0	0.4	0.6	0.8	0.9
0.1	2	0	0.3		2.845 61	1.207 28	0.837 85	0.550 33	0.385 38
		0.6			2.829 62	1.180 81	0.799 36	0.483 24	0.295 52
		1.2			2.813 74	1.156 66	0.766 76	0.436 66	0.248 75
		1.6			2.803 25	1.141 68	0.747 65	0.413 02	0.228 54

ϕ	K	M_2	Ec	S	A	0	0.4	0.6	0.8	1
0.1	0.3	0	0.5	0.3		2.590 80	2.631 42	2.681 49	2.765 09	2.967 22
		1				2.300 28	2.323 87	2.350 76	2.388 98	2.435 92
		2				2.042 29	2.054 82	2.067 78	2.082 85	2.090 71
		3				1.808 66	1.813 46	1.817 18	1.818 22	1.806 90

porous medium causes higher restriction to the fluid flow which, in turn, retards the fluid velocity, and due to which there is increase in the temperature. Figure 8 is prepared to analyze the effect of the Prandtl number on temperature field. It is seen that the temperature and the thermal boundary layer thickness decreases effectively with an increment in the Prandtl number. Physically it signifies that an increase in the Prandtl number means an increase of fluid viscosity, which causes a decrease in the temperature distribution. The influence of the magnetic parameter on the temperature field is portrayed in figure 9. It is observed that with an increment in the magnetic parameter the fluid energy increases significantly. Actually, magnetic parameter strongly depends upon the Lorentz force. The higher magnetic parameter has the stronger Lorentz force and the lower magnetic parameter

corresponds to the weaker Lorentz force. The stronger Lorentz force generates more heat in the fluid motion which shows an increment in the temperature and thermal boundary layer thickness. The variations of the solid volume fraction with combine effect of the suction/injection parameter is plotted on the temperature field in figure 10. It is seen that with an increase in the solid volume fraction the fluid temperature increases for suction and decreasing trend is noticed for the injection parameter. The behavior of the velocity ratio parameter on the temperature field is plotted in figure 11. The fluid temperature decreases effectively with an increase in the velocity ratio parameter.

To capture the heat transfer rate, the local Nusselt number is plotted against the variations in the Eckert number, the magnetic parameter, the permeability parameter and the

Table 6. Numerical values of the local Nusselt number $-\theta'(0)$ for $Ec = 0.3, m = 4.9, Pr = 6.2$ and $N = 0.5$.

ϕ	A	M_2	S	K	0	0.3	0.5	0.6	0.7	
0	0.1	2	0.3		2.845 61	2.837 61	2.832 29	2.829 62	2.826 97	
0.1					2.150 82	2.140 93	2.134 44	2.131 23	2.128 04	
0.2					1.679 77	1.668 83	1.661 72	1.658 21	1.654 74	
0.2			-1		0.763 47	0.748 58	0.738 44	0.733 30	0.728 12	
			-0.5		0.982 01	0.964 36	0.952 65	0.946 82	0.941 00	
			0		1.369 28	1.355 42	1.346 37	1.341 90	1.337 47	
			0.5		1.913 54	1.904 38	1.898 42	1.895 49	1.892 59	
			1		2.570 09	2.564 36	2.560 64	2.558 80	2.556 99	
A	M_2	K	S	ϕ	0	0.4	0.6	0.8	0.9	
0.1	2	0	0.3		2.845 61	1.094 03	0.748 79	0.494 69	0.351 28	
		0.6			2.829 62	1.067 54	0.710 25	0.425 92	0.258 79	
		1.2			2.813 74	1.043 58	0.678 26	0.380 91	0.215 13	
		1.6			2.803 25	1.028 82	0.659 76	0.358 65	0.196 79	
ϕ	K	M_2	Ec	S	A	0	0.4	0.6	0.8	1
0.1	0.3	0	0.5	0.3		2.492 60	2.533 32	2.583 55	2.667 47	2.870 37
		1				2.213 31	2.237 41	2.264 99	2.304 52	2.354 25
		2				1.965 54	1.978 82	1.992 78	2.009 61	2.020 79
		3				1.741 36	1.747 07	1.751 97	1.755 01	1.747 19

Table 7. Numerical values of the local Nusselt number $-\theta'(0)$ for $Ec = 0.3, m = 5.7, Pr = 6.2$ and $N = 0.5$.

ϕ	A	M_2	S	K	0	0.3	0.5	0.6	0.7	
0	0.1	2	0.3		2.845 61	2.837 61	2.832 29	2.829 62	2.826 97	
0.1					2.098 27	2.088 26	2.081 70	2.078 45	2.075 22	
0.2					1.612 63	1.601 61	1.594 45	1.590 92	1.587 43	
0.2			-1		0.744 35	0.728 76	0.718 13	0.712 75	0.707 33	
			-0.5		0.952 56	0.934 70	0.922 87	0.916 98	0.911 11	
			0		1.319 60	1.305 66	1.296 57	1.292 08	1.287 64	
			0.5		1.832 96	1.823 70	1.817 69	1.814 73	1.811 80	
			1		2.451 36	2.445 52	2.441 73	2.439 86	2.438 01	
A	M_2	K	S	ϕ	0	0.4	0.6	0.8	0.9	
0.1	2	0	0.3		2.845 61	1.030 73	0.700 34	0.464 74	0.333 06	
		0.6			2.829 62	1.004 34	0.662 00	0.395 46	0.239 61	
		1.2			2.813 74	0.980 60	0.630 55	0.351 60	0.197 84	
		1.6			2.803 25	0.966 04	0.612 49	0.330 23	0.180 56	
ϕ	K	M_2	Ec	S	A	0	0.4	0.6	0.8	1
0.1	0.3	0	0.5	0.3		2.432 02	2.472 79	2.523 12	2.607 25	2.810 62
		1				2.159 61	2.184 01	2.212 02	2.252 35	2.303 80
		2				1.918 10	1.931 84	1.946 40	1.964 30	1.977 52
		3				1.699 70	1.705 97	1.711 58	1.715 84	1.710 17

suction/injection see figures 12–15. It is seen that the Nusselt number is directly proportional to the Eckert number, the magnetic parameter and the permeability parameter. Figure 15 shows that for the injection parameter the heat transfer rate is high as compared to the suction parameter. It is noticed through figure 16, that the local skin friction coefficient is decreased for the mass suction parameter and increased for the mass blowing parameter. In figure 17, the local skin friction coefficient is observed to grow gradually

with an increment in the solid volume fraction. A decrement in the local skin friction coefficient for the increasing values of the Hartmann number is concluded through figure 18.

Table 1, represents the thermophysical properties of the base fluid (water) and nanoparticles (copper). Table 2 deals the numerical values of nanoparticle shape factor m . Results for code verification are presented in table 3. Table 4 display the values of the local skin friction $f''(0)$. The values of local Nusselt number $-\theta'(0)$ owing the different emerging

parameters for different shape factors of nanoparticles shown in tables 5–7. Furthermore, the negative amount of the local skin friction in table 4 describe the effect of the drag force on the sheet.

5. Conclusion

This article examined the radiative and hydromagnetic nanofluid flow with the suction/injection effects over an exponentially stretching surface. The main findings of the analysis have been wrapped up in the following text:

- The velocity profile is an increasing function of the solid volume fraction, velocity ratio parameter and the mass blowing whereas it has an opposite behavior for the mass suction parameter.
- The temperature profile accelerates with the growth of the Eckert and Hartmann numbers.
- It is seen that the temperature field decreases by increasing the Prandtl number and the velocity ratio parameter.
- An increment in the suction parameter is found responsible for an augmentation in the rate of heat transfer.
- The impact of shape factor for Platelets is greater than that of cylinder and bricks against temperature variation.
- Nusselt number is the increasing function of Eckert number, magnetic parameter and permeability parameter.
- Local skin friction coefficient increase with an increase in the solid volume fraction factor.

References

- [1] Choi S U S 1995 Enhancing thermal conductivity of fluids with nanoparticles *Proc. of the ASME Int. Mechanical Engineering Congress and Exposition* vol 66 (San Francisco, USA) (New York: ASME) pp 99–105
- [2] Wang X, Xu X and Choi S U S 1999 Thermal conductivity of nanoparticle fluid mixture *J. Thermophys. Heat Transfer* **13** 474–80
- [3] Buongiorno J 2006 Convective transport in nanofluids *ASME J. Heat Transfer* **128** 240–50
- [4] Kiblinki P, Phillpot S R, Choi S U S and Eastman J A 2002 Mechanism of heat flow in suspensions of nano-sized particles (nanofluids) *Int. J. Heat Mass Transfer* **42** 855–63
- [5] Eastman J A, Choi S U S, Li S, Yu W and Thompson L J 2001 Anomalous increased effective thermal conductivity of ethylene glycol-based nanofluids containing copper nanoparticles *Appl. Phys. Lett.* **78** 718–20
- [6] Nield D A and Kuznetsov A V 2009 The Cheng-Minkowycz problem for natural convective boundary-layer flow in a porous medium saturated by a nanofluid *Int. J. Heat Mass Transfer* **52** 5792–5
- [7] Kakac S and Pramuanjaroenkij A 2009 Review of convective heat transfer enhancement with nanofluids *Int. J. Heat Mass Transfer* **52** 3187–96
- [8] Srinivas T and Vinod A V 2015 Heat transfer enhancement using CuO/water nanofluid in a shell and helical coil heat exchanger *Proc. Eng.* **127** 1271–7
- [9] Hassani M, Tabar M M, Nemati H, Domairry G and Noori F 2011 An analytical solution for boundary layer flow of a nanofluid past a stretching sheet *Int. J. Therm. Sci.* **50** 2256–63
- [10] Rana P and Bhargava R 2012 Flow and heat transfer of a nanofluid over a nonlinearly stretching sheet: a numerical study *Commun. Nonlinear Sci. Numer. Simulat.* **17** 212–26
- [11] Khan W A and Pop I 2010 Boundary-layer flow of a nanofluid past a stretching sheet *Int. J. Heat Mass Transfer* **53** 2477–83
- [12] Hamad M A A and Ferdows M 2012 Similarity solution of boundary layer stagnation-point flow towards a heated porous stretching sheet saturated with a nanofluid with heat absorption/generation and suction/blowing: a Lie Group analysis *Commun. Nonlinear Sci. Numer. Simulat.* **17** 132–40
- [13] Sun C, Lu W Q, Bai B and Liu J 2011 Anomalous enhancement in thermal conductivity of nanofluid induced by solid walls in a nanochannel *Appl. Therm. Eng.* **31** 3799–805
- [14] Nam J S, Lee P H and Lee S W 2011 Experimental characterization of micro-drilling process using nanofluid minimum quantity lubrication *Int. J. Mach. Tool. Manu.* **51** 649–52
- [15] Sheikholeslami M, Ganji D D and Rashidi M M 2016 Magnetic field effect on unsteady nanofluid flow and heat transfer using Buongiorno model *J. Magn. Magn. Mater.* **416** 164–73
- [16] Sheikholeslami M and Ganji D D 2016 Nanofluid convective heat transfer using semi analytical and numerical approaches: a review *J. Taiwan Inst. Chem. Eng.* **64** 43–77
- [17] Crane L 1970 *J. J. Appl. Math. Phys. (ZAMP)* **21** 645
- [18] Andersson H I 1995 An exact solution of the Navier–Stokes equations for magnetohydrodynamic flow *Acta Mech.* **113** 241–4
- [19] Wang C Y 2009 Analysis of viscous flow due to a stretching sheet with surface slip and suction *Nonlinear Anal.: Real World Appl.* **10** 375–80
- [20] Andersson H I 2002 Slip flow past a stretching surface *Acta Mech.* **158** 121–5
- [21] Fang T, Zhang J and Yao S 2009 Slip MHD viscous flow over a stretching sheet: an exact solution *Commun. Nonlinear Sci. Numer. Simulat.* **14** 3731–7
- [22] Alinejad J and Samarbaksh S 2012 Viscous flow over nonlinearly stretching sheet with effects of viscous dissipation *J. Appl. Math.* **2012** 587834
- [23] Kumbhakar B and Rao P S 2015 Dissipative boundary layer flow over a nonlinearly stretching sheet in the presence of magnetic field and thermal radiation *Proc. Natl. Acad. Sci. A* **85** 117–25
- [24] Seth G S and Mishra M K 2016 Analysis of transient flow of MHD nanofluid past a non-linear stretching sheet considering Navier’s slip boundary condition *Adv. Powder Technol.* **28** 375–84
- [25] Jayarami R K, Madhusudhana N P and Konijeti R 2018 MHD mixed convection flow of radiating and chemically reactive Casson nanofluid over a nonlinear permeable stretching sheet with viscous dissipation and heat source *Multidiscip. Model. Mater. Struct.* **14** 609–30
- [26] Magyari E and Keller B 1999 Heat and mass transfer in the boundary layers on an exponentially stretching continuous surface *J. Phys. D: Appl. Phys.* **32** 577–85
- [27] Elbashbeshy E M A 2001 Heat transfer over an exponentially stretching continuous surface with suction *Arch. Mech.* **53** 643–51

- [28] El-Aziz M A 2009 Viscous dissipation effect on mixed convection flow of a micropolar fluid over an exponentially stretching sheet *Can. J. Phys.* **87** 359–68
- [29] Mandal I C and Mukhopadhyay S 2013 Heat transfer analysis for fluid flow over an exponentially stretching porous sheet with surface heat flux in porous medium *Ain Shams Eng. J.* **4** 103–10
- [30] Bilal S, Malik M Y, Awais M, Rehman K, Hussain A and Khan I 2017 Numerical investigation on 2D viscoelastic fluid due to exponentially stretching surface with magnetic effects: an application of non-Fourier flux theory *Neural. Comput. Appl.* **30** 2749–58
- [31] Chakrabarti A and Gupta A S 1979 Hydromagnetic flow and heat transfer over a stretching sheet *Quart. Appl. Math.* **37** 73
- [32] Abramowitz M and Stegun L A 1972 *Handbook of Mathematical Functions* vol 55 (Gaithersburg, MD: National Bureau of Standards)
- [33] Timofeeva E V, Routbort J L and Singh D 2009 Particle shape effects on thermophysical properties of alumina nanofluids *J. Appl. Phys.* **106** 014304
- [34] Bhattacharyya K, Uddin M S and Layek G C 2016 Exact solution for thermal boundary layer in Casson fluid flow over permeable shrinking sheet with variable wall temperature and thermal radiation *Alexandria Eng. J.* **55** 1703–12